Defence Technology 14 (2018) 83–92

Contents lists available at ScienceDirect

Defence Technology

journal homepage: www.elsevier.com/locate/dt

Evaluating location specific strain rates, temperatures, and accumulated strains in friction welds through microstructure modeling

Javed Akram [a], Prasad Rao Kalvala [a, *], Vikas Jindal [b], Mano Misra [a]

[a] Dept. of Metallurgical Engineering, University of Utah, Salt Lake City, UT 84112, USA
[b] Dept. of Metallurgical Engineering, Indian Institute of Technology (BHU), Varanasi, India

ARTICLE INFO

Article history:
Received 30 August 2017
Received in revised form
9 October 2017
Accepted 3 November 2017
Available online 6 November 2017

Keywords:
Microstructure modeling
Dynamic recrystallization
Friction welding
Inconel 718
EBSD
Hot deformation
Strain map

ABSTRACT

A microstructural simulation method is adopted to predict the location specific strain rates, temperatures, grain evolution, and accumulated strains in the Inconel 718 friction welds. Cellular automata based 2D microstructure model was developed for Inconel 718 alloy using theoretical aspects of dynamic recrystallization. Flow curves were simulated and compared with experimental results using hot deformation parameter obtained from literature work. Using validated model, simulations were performed for friction welds of Inconel 718 alloy generated at three rotational speed i.e., 1200, 1500, and 1500 RPM. Results showed the increase in strain rates with increasing rotational speed. These simulated strain rates were found to match with the analytical results. Temperature difference of 150 K was noticed from center to edge of the weld. At all the rotational speeds, the temperature was identical implying steady state temperature ($0.89T_m$) attainment.

1. Introduction

Friction based welding processes such as friction welding and friction stir welding are widely used for joining similar and dissimilar metals. These welds are not subjected to melting and solidification [1–4] compared to conventional fusion based processes. Many problems such as hot cracking, porosity, inclusion, and dilution which are characteristic features of fusion welding are absent in the friction based welding processes. In both fusion [5] and solid-state welding [6] methods, exposure to high temperature results in heterogeneous microstructure across the weldment. In fusion welding, parameters influencing the microstructure are thermal related such as thermal gradient and cooling rate. However, in solid state welds, the microstructural changes across the weldment are influenced not only by temperature but pressure too. For example, the weldment of fusion welded sample consists of solidified columnar grains followed by coarse grain heat affected zone (CGHAZ), fine grain heat affected zone (FGHAZ), inter-critical heat affected zone (ICHAZ), and unaffected zone of base metal [7]. In contrast, the friction stir and friction welded weldment consists of a weld interface of very fine grain structure followed by thermo-mechanically heat affected zone (TMHAZ) [1–3,8]. The width of refined grain zone in friction stir welding is relatively larger while it is smaller in a friction weld. The formation of the refined grain structure at the weld interface or stir zone is attributed to dynamic recrystallization (DRX) phenomena due to high strain rate and temperature involvement. In these methods, friction between two metals generates heat and combination of applied pressure and rotational speed generates high strain rate in the system. Therefore, microstructural evolution in friction based methods is dictated by different strain rates and temperatures exposures across the weldment. However, prediction of these parameters by experimental route is very complicated, especially strain rates and temperatures. For friction stir welding, various modeling approaches were taken to predict the thermal profiles, metal flow behavior, strain rates [9–12] and microstructural evolution [13–15] across the weldment. As for friction welds, not much attention is paid to modeling area except few numerical studies [16]. In view of the

* Corresponding author. 135 S 1460 E Rm 412, Department of Metallurgical Engineering, University of Utah, Salt Lake City, UT 84112, USA.
E-mail address: Prasad.Kalvala@utah.edu (P.R. Kalvala).
Peer review under responsibility of China Ordnance Society.

https://doi.org/10.1016/j.dt.2017.11.002

limited understanding of microstructural aspects of friction based welds through theoretical understanding, this work was taken up. It is aimed to predict the strain rates, temperatures, and microstructural evolution during friction welding through microstructural modeling route using theoretical aspects of dynamic recrystallization.

For modeling of DRX, several methods have been adopted such as Monte Carlo [17], phase field [18], and cellular automata [19,20] methods. Among these, cellular automata method gained much attention for microstructural modeling of DRX due to its discrete temporal evolution of space and time. Thus, cellular automata method is adopted in the present work. First part of the work is focused on DRX modeling and its validation with the experimental data of super alloy Inconel 718 during hot compression [21] taken from literature and second part is focused on using the validated model to predict the strain rates, temperatures, induced strain, and microstructural evolution during friction welding of Inconel 718 carried out in the present study by our group.

Inconel alloys are widely used for military aircraft applications to withstand a combination of high temperature, hot gas corrosion and high strength. Inconel 718 is an established alloy for commercial and military aircraft airframe and engine components. The outcome of this study would help enhance the understanding of microstructure evolution and mechanical response of Inconel 718 super alloy during friction welding as well as during any hot deformation process. Prior prediction/knowledge of these results would be useful for controlling the final microstructure and deciding the post processing treatment conditions for achieving the final property of a material.

2. Background

2.1. Cellular automata method

Cellular automata [15] is an algorithm where space of interest is divided into finite number of grids called as 'cells'. The state of a cell is governed by its local neighborhood and the transformation rule. There are two types of neighborhood which can be used for simulation of recrystallization i.e., von Neumann's and Moore's neighborhood. In von Neumann's only nearest neighbors are considered whereas Moore's consider both nearest and secondary neighbors. The state of any cell at time step $(t+\Delta t)$ using von Neumann's neighboring rule can be expressed as

$$\xi_{i,j}^{t+\Delta t} = f\left(\xi_{i-1,j}^{t}, \xi_{i,j-1}^{t}, \xi_{i,j}^{t}, \xi_{i+1,j}^{t}, \xi_{i,j+1}^{t}\right) \tag{1}$$

where $\xi_{i,j}^{t}$ represents the value of variables ξ at site (i,j) at time t. Function f is the transformation rule which determines the evolution of the site (i,j) along with time, and it can be set according to the characteristics of the system of interest.

2.2. Theoretical model & simulation procedure for DRX

Dynamic recrystallization (DRX) is commonly observed in metals when subjected to high temperature deformation. Mostly low to medium stacking fault energy system show this kind of behavior such as copper and nickel based alloys. DRX is known to occur when dislocation density of the system reaches to some critical value which, in turn, depends on high temperature deformation parameters such as strain rate and temperature [22]. The final microstructure of DRX depends on two important phenomena; nucleation and growth. Both nucleation and growth are closely related to dislocation density.

For this work, 2D square lattice was employed. Four state variables were allocated to each of the cells; (i) grain number represents different grains, (ii) grain color represents orientation and boundary energy of the grain, (iii) dislocation density variable and (iv) distance variable which controls the grain growth. Von Neumann's neighborhood was used to simulate the grain growth.

For the evolution of dislocation density Estrin and Mecking law [23] was used. Based on this law, the dependence of dislocation density with strain can be expressed as

$$\frac{\mathrm{d}\rho}{\mathrm{d}\varepsilon} = k_1 - k_2\rho \tag{2}$$

where k_1 is the constant that represents hardening and k_2 is the recovery parameter. The constant k_1 is independent of strain rate and only depends on temperature whereas recovery parameter k_2 is a function of both strain rate and temperature. The high temperature flow stress at the macroscopic level can be calculated using following expression which is related to the dislocation density [24,25].

$$\sigma = \alpha G b\sqrt{\rho} \tag{3}$$

where α is the dislocation interaction term (typically ranges from 0.5 to 1.0 for most of the metals), G is the shear modulus of the material, b is the burgers vector, and $\sqrt{\rho}$ is the mean dislocation density, given by

$$\overline{\rho} = \frac{1}{n}\sum_{i=1}^{n}\rho_i \tag{4}$$

where n is the total number of cells and ρ_i is the dislocation density of ith cell. k_1 is related with the hardening rate [22] and expressed as

$$\theta_0 = \alpha G b k_1/2 \tag{5}$$

where θ_0 is the hardening rate and can be determined from the slope of experimental flow curve at particular temperature. The recovery parameter k_2 and hardening constant (k_1) [22] are related with each other as follows

$$\sigma_s = \alpha G b k_1/k_2 \tag{6}$$

where σ_s is the steady state stress. The recovery parameter k_2 can be determined after calculating the value of k_1 and σ_s. The steady state stress [26] is calculated according to the following equation

$$\sigma_s = \frac{1}{\alpha}\sinh^{-1}\left(\frac{Z}{A}\right)^{\frac{1}{n}} \tag{7}$$

where $A, \alpha,$ *and* n are the material constants. Z is the Zener Holloman parameter which is a function of strain rate and temperature and given by following equation

$$Z = \dot{\varepsilon}\exp\left(\frac{Q_{act}}{RT}\right) \tag{8}$$

where $\dot{\varepsilon}$ is the strain rate, T is the temperature in Kelvin and R is the gas constant. In the beginning of the deformation, evolution of dislocation with strain was calculated using equation (2). Once the dislocation of the deforming matrix crosses the critical value of the dislocation, new nuclei will form at the grain boundary. The value of the critical dislocation density can be calculated using following expression derived by Roberts and Ahlblom [27].

$$\rho_c = \left(\frac{20\gamma_i \dot{\varepsilon}}{3blM\tau^2}\right)^{1/3} \quad (9)$$

where γ_i is the grain boundary energy, M is the grain boundary mobility, l is the dislocation mean free path and τ is the dislocation line energy and can be calculated from the following expression [24].

$$\tau = 0.5Gb^2 \quad (10)$$

In the present study, nucleation rate is calculated based on following equation which is function of both strain rate and temperature [22].

$$\dot{n}(\dot{\varepsilon}, T) = C\dot{\varepsilon}^m \exp\left(-\frac{Q_{act}}{RT}\right) \quad (11)$$

where C is the nucleation constant and m is the exponent which is set to 1 in this study. For a specific hot deformation condition, if the percentage of DRX and grain size is known, nucleation rate can be calculated using equation (12) [22].

$$\eta = \dot{n}\frac{\varepsilon}{\dot{\varepsilon}}\frac{4}{3}\pi r^3 \quad (12)$$

where η is the percentage of DRX, ε is the true strain and r is the mean radius of recrystallized grain. Once the nuclei are generated at the grain boundary or any defected area that cell is considered as recrystallized cell. The dislocation density of that cell is set to zero or annealed state dislocation density which raises the difference in dislocation densities between deformed and recrystallized cells. The difference in dislocation densities generates a force for the nuclei to grow. The velocity of the grain follows the following equation [20,22].

$$V = M\Delta f \quad (13)$$

where Δf is the driving force per unit area and M is the grain boundary mobility which can be calculated as follows

$$M = M_0 \exp\left(\frac{-Q_b}{RT}\right) \quad (14)$$

where M_0 is the constant and Q_b is the boundary diffusion activation energy. The driving force is a function of dislocation density difference and grain boundary energy, expressed as [20,22].

$$\Delta f = \tau(\rho_m - \rho_i) - \frac{2\gamma_i}{r_i} \quad (15)$$

where γ_i is the grain boundary energy which is a function of grain boundary misorientation (θ). It can be calculated from Read–Shockley equation [20,22].

$$\gamma_i = \gamma_m \frac{\theta_i}{\theta_m}\left(1 - \ln\left(\frac{\theta_i}{\theta_m}\right)\right) \quad (16)$$

where γ_m and θ_m are the grain boundary energy and mean misorientation angle, respectively. $\gamma_i = \gamma_m$ when misorientation angle 'θ' is higher than 15°.

The initial microstructure was created by populating fixed number of nuclei in a matrix and allowed them to grow until it impinges with each other. The orientation of the grains was selected randomly and ranges from 1 to 180°. Fig. 1 represents the initial microstructure created as described above. The matrix consists of 250×250 cells. Each cell in real dimension is equivalent to 1 μm. Periodic boundary conditions were used for this simulation. Time step Δ t is calculated as $\frac{d}{v_{max}}$, where d is the diameter of critical radius and v_{max} is the maximum velocity. Table 1 shows the constants used for this simulation. All the constant values were calculated using experimental data from Chen et al. work [21].

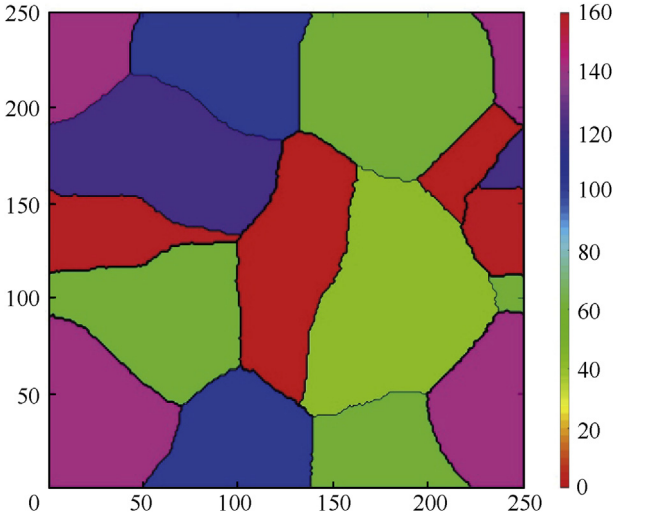

Fig. 1. Initial microstructure generated by cellular automata. Color represents orientation of a grain.

3. Material and methods

The chemical composition (wt%) of Inconel alloy 718 rod (16.5 mm diameter) that was used for friction welding is as follows: 51.6% Ni, 18.2% Cr, 5.1% Nb, 3.28% Mo, 1.06% Ti, 0.56% Al, 0.33% V, 0.09% Mn, 0.01% S, 0.004% C, 0.003% B and 19.793% Fe. The microstructure of as received Inconel 718 is shown in Fig. 2. Microstructure consists of equiaxed grains and annealing twins with an average grain size of 29 μm. Rotary friction welding machine was used to develop friction welds. Following welding parameters were used: Friction Pressure: 300 MPa, Upset Pressure: 600 MPa, Burn-off length: 4 mm, and Rotational Speeds of 1200, 1500, and 1800 RPM.

Microstructural analysis of as received and welded samples was performed with optical and scanning electron microscope. Standard metallographic procedure of hot mounting, grinding, and polishing were performed to prepare the sample upto the surface roughness of 0.05 μm followed by etching. Samples were etched using balling reagent (100 ml ethanol + 100 ml HCl + 5 g $CuCl_2$). For electron backscattered diffraction (EBSD) studies, samples were prepared by mechanical polishing followed by final polishing with diamond and colloidal silica for 4 h. EBSD studies were conducted using an FEI Quanta-600 scanning electron microscope (SEM) equipped with TSL-OIM software with a step size of 1 μm. Linear intercept method is used to calculate the simulated grain size.

4. Results & discussion

4.1. Model validation

The experimental results mentioned in this section to compare with our simulated results are referred from literature [21]. A typical flow curve during high temperature deformation consists of three stages: work hardening, softening and steady state stage. In work hardening stage, the accumulation of dislocation is very high due to weak recovery leading to accelerated increase in the flow

Table 1
Constant values used for the simulation of Inconel 718 alloy [21].

G/Pa	b/m	γ/(J·m^2)	Q_{act}/(kJ·mol^{-1})	Q_b /(kJ·mol^{-1})	n	α	A/Pa$^{1/n}$
8.31×10^{10}	2.56×10^{-10}	0.625	474	474	4.2	0.00415	7.07×10^{17}

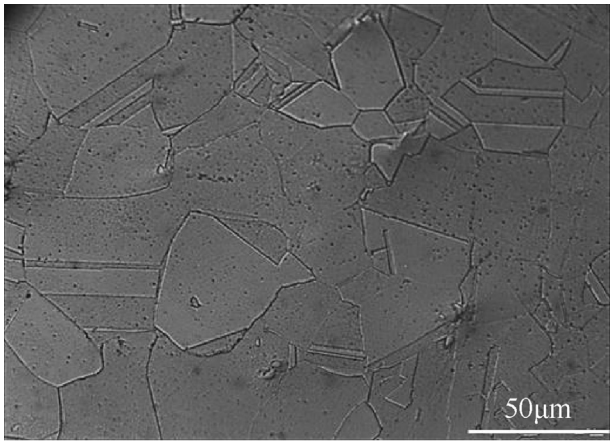

Fig. 2. As received base metal microstructure of Inconel 718.

stress. Once the dislocation reaches a critical value, dynamic recrystallization takes place resulting in dislocation annihilation which reduces the flow stress of the material (softening stage). In the steady stage region, dynamic balance reaches between dislocation accumulation (work hardening) and dislocation annihilation. Fig. 3(a) represents the simulated and experimental flow curves [21] at constant temperature (1253 K) with different strain rates (1, 0.1, 0.01, and 0.001s^{-1}). Similarly, Fig. 3(b) shows the simulated and experimental flow curves [21] at constant strain rate (1 s^{-1}) with different temperatures (1193, 1223, 1253, 1283, and 1313 K).

Increasing trend in flow stress was observed at high strain rates and low deformation temperature which can be attributed to (1) higher rate of dislocation accumulation and (2) low rate of recrystallization. At higher strain rate, the rate of dislocation accumulation is fast which leads to high amount of work hardening into the system. Further, the deformation time is short as compared to lower strain rates thus reduces the growth of new recrystallized grains. On the other hand, at high temperature, the mobility of growing grain is faster which annihilates the dislocations generated by work hardening thus reducing the flow stress of the system. Simulated results are found to agree well with the experimental results as shown in Fig. 3(a) and (b). All the simulated peak stress values are quite comparable with the experimental peak stress values.

Small deviation has been observed at later stages of the deformation after 0.5% of true strain. This deviation is observed when it is deformed at high strain rates or at lower temperatures. It is found that adiabatic heating also plays a role in softening of material apart from dynamic recrystallization when deformed under high strain rates and lower temperatures as reported by Weis et al., [28]. It has been reported that adiabatic heating increased the temperature of the system by 333 K when deformed at 1223 K and a strain rate of 1 s^{-1}. In the present model, flow curves were simulated using constant temperature, therefore, it can be concluded that deviation from experimental flow curves in later stages of deformation is due to increased temperature (ΔT) in the system due to adiabatic heating. Apart from flow curve, the model is also validated with reported grain size. Fig. 4 shows the simulated microstructures at different temperatures (a) 1223 K (b) 1253 K and (c) 1283 K while keeping the strain rate constant (0.001s^{-1}). Fig. 5 shows the simulated microstructures at different strain rates (a) 0.1 s^{-1}(b) 0.01s^{-1}and (c) 0.001s^{-1} keeping the deformation temperature (1313 K) constant. The simulated microstructure agreed well with the experimental results reported by X. M. Chen et al. [21] as listed in Table 2. In micrograph, each color represents the orientation of a grain. The results indicate the closeness of experimental and simulated results. Further, this validated model is used to predict the strain rates and temperatures exposures in friction welds and covered in following section.

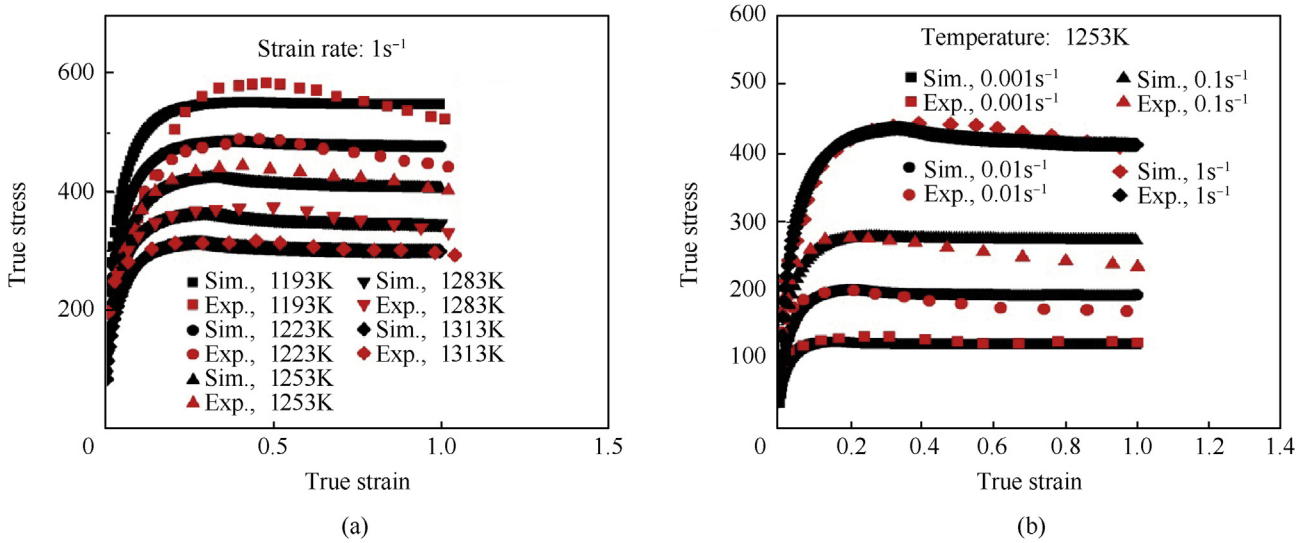

Fig. 3. Comparison of experimental [21] and simulated flow curve (a) for different temperatures 1193, 1223, 1253, 1283, and 1313 K) keeping constant strain rate of 1s^{-1} and (b) for different strain rates (0.001, 0.01, 0.1, and 1s^{-1}) keeping constant temperature of 1253 K.

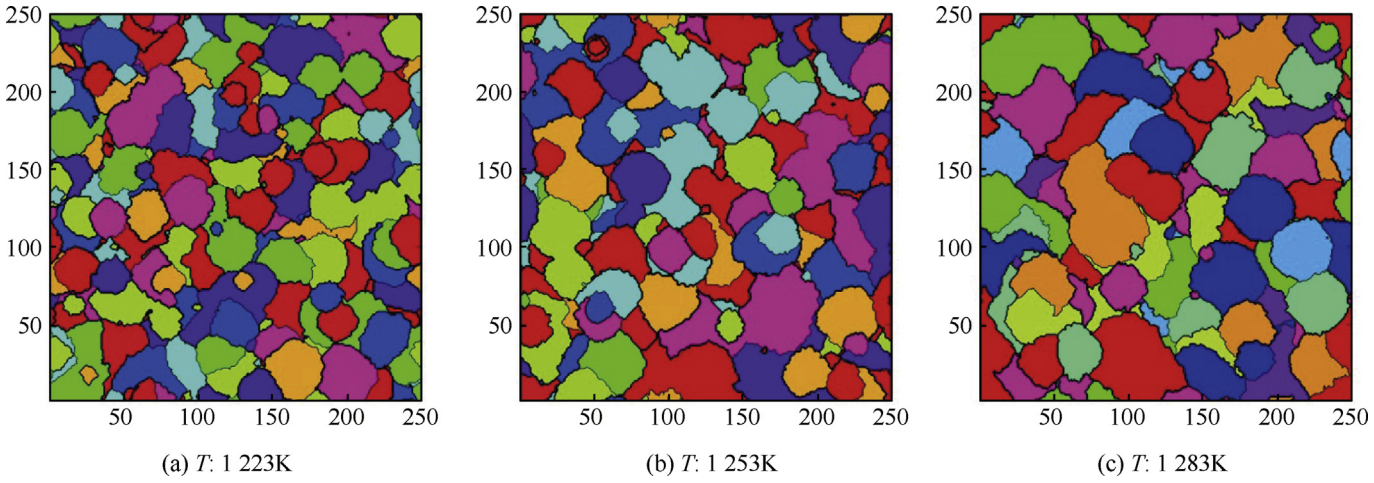

Fig. 4. Simulated microstructures at different temperatures (a) 1223 K (b) 1253 K and (c) 1283 K with constant strain rate of 0.001s^{-1}.

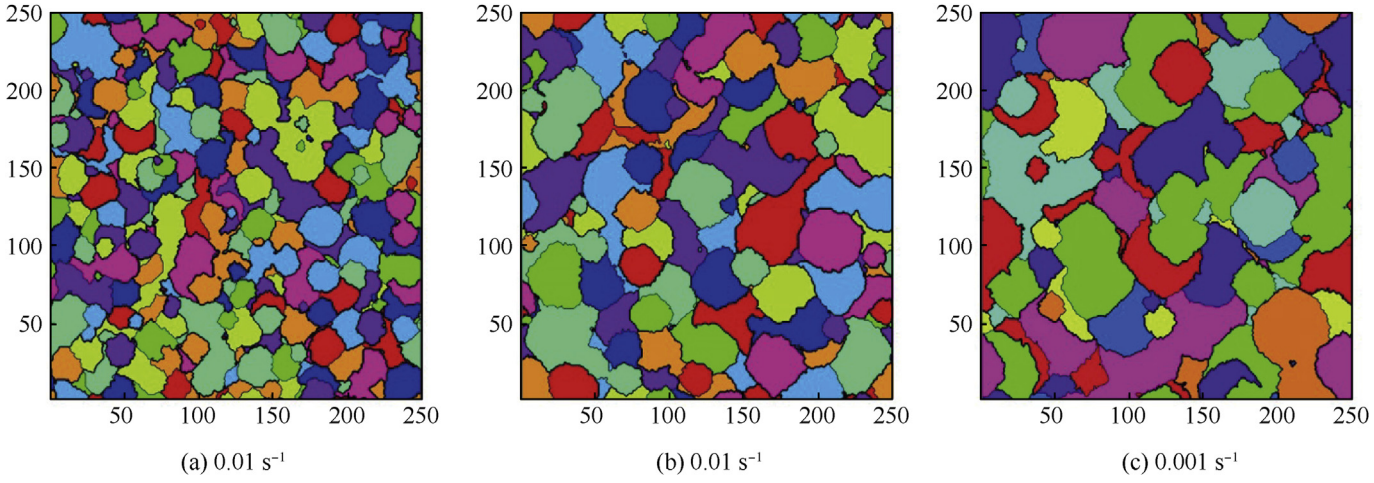

Fig. 5. Simulated microstructures at different strain rates (a) 0.1 s^{-1}(b) 0.01$s^{-1}$and (c) 0.001s^{-1} with constant temperature of 1313 K.

Table 2
List of grain size values from experiment [21] and simulation at different strain rates and temperature. Simulated grain size is average of three simulation results.

Temperature/K	1223	1253	1283	1313		
Strain rate/s^{-1}	0.001			0.1	0.01	0.001
Experimental grain size/μm	11.3	14.1	17.6	10.2	14.2	18.8
Simulated grain size/μm	11.89 ± 0.28	14.3 ± 0.12	16.75 ± 0.42	10.02 ± 0.56	13.8 ± 0.46	18.8 ± 0.29

4.2. Prediction of strain rate and temperature in friction welds using grain size

To study the grain evolution, strain rates, and temperature exposures in friction welds of Inconel 718, three welds were generated at different rotational speeds i.e., 1200, 1500, and 1800 RPM. Fig. 6 show the cross-sectional view of a typical friction weld developed at 1500 RPM. The welded region has shape like lens (marked with red color in Fig. 6) which is mostly composed of very fine equiaxed grains and can be differentiated in the picture by the white region. The formation of refined grains in the welded region is due to involvement of very high strain rates and temperature. Grain refinement phenomena due to involvement of high strain rates and temperatures are commonly known as dynamic recrystallization [29,30]. Fig. 7 shows the EBSD map from center and edge location of friction weld sample welded at 1500 RPM. Fig. 7(a) and (b) corresponds to edge and center location of the weld, respectively. It can be seen from Fig. 7 that the grain size at both location

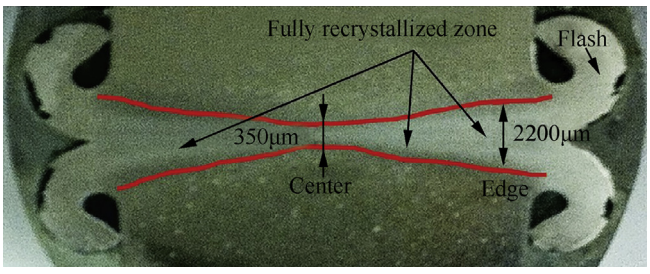

Fig. 6. Cross section view of friction weld of Inconel 718 generated with 1500 RPM.

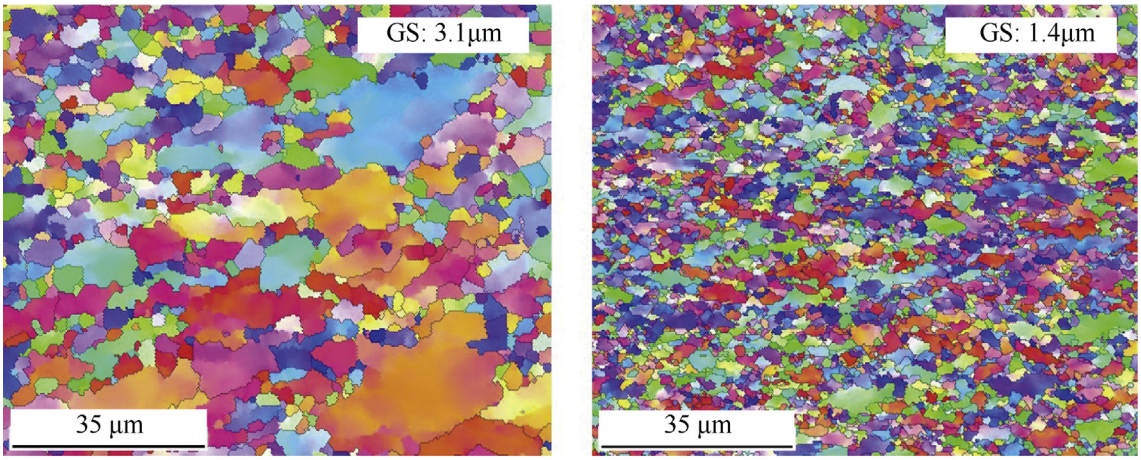

Fig. 7. EBSD pattern of Inconel 718 friction weld developed with 1500 RPM (a) at edge (b) at weld center.

of the weld went through significant size reduction as compared to their base counterpart. For example, the average grain size at the center and edge of a welded sample was found to be 1.4 and 3.1 μm, respectively. Although, they showed significant size reduction compared with base material, they also show different grain sizes compared with each other. The difference in grain sizes at these two regions could be attributed to different strain rate and temperature exposure. Fig. 8 shows the temperature profile captured by IR camera on the outer surface of the IN 718 rod during friction welding performed using 1500 RPM. The maximum temperature recorded by IR camera was found to be 1473 K. By assuming similar temperatures at both center and edge of the weld for a particular rotation speed, the only parameter which creates the difference in grain size will be strain rate. Afterward, the validated model is used to predict the strain rate experienced during welding. For that, the temperature was kept constant equal to recorded one (1473 K) and strain rates were varied till the grain size matched with the experimental values.

At strain rate of 294 s^{-1}, the simulated grain size which is 2.97 μm (Fig. 9(a) matched very close to the value (3.1 μm) obtained from experiment as shown in Fig. 7(a). Similarly, by assuming that

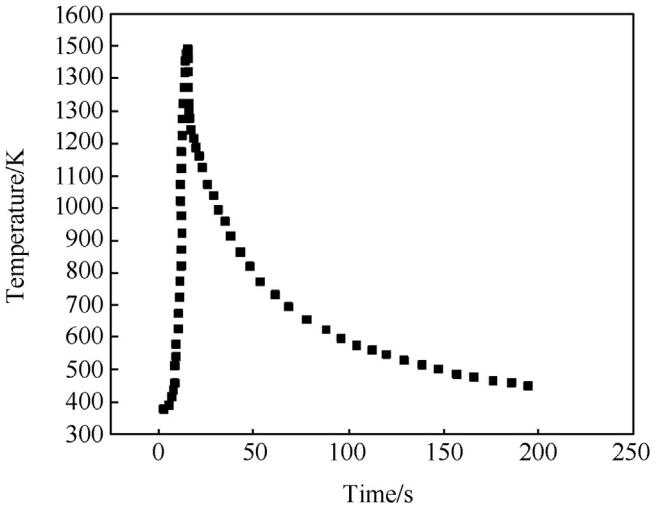

Fig. 8. Temperature profile recorded by IR camera during friction welding performed at 1500 RPM.

the temperature experienced at the contact zone is similar though out the radial direction, a strain rate of 1850 s^{-1} is obtained which matched the experimental grain size values which is 1.4 μm (Fig. 7(b)). The predicted strain rate at the center of weld is higher than the edge of the weld which is not feasible because radial velocity always increases towards periphery. O. T. Midling and O. Grong [16] showed effective strain rate (radial, axial, and rotational) increases with radial position, means periphery attain higher effective strain rate compared to the center of a rod during friction welding of aluminum alloys which is contradictory to our finding. This suggests that not only the strain rate but temperature is also different at the center of weld compared with edge. To predict the temperature variation, analytical approach is taken to first identify the strain rate during welding as adopted by Chang et al. [31,32], for friction stir welding. The material flow strain rate ($\dot{\varepsilon}$) during friction welding can be derived by the torsion type deformation as

$$\dot{\varepsilon} = \frac{R_m 2\pi r_e}{L_e} \tag{17}$$

where R_m is the average material flow rate which is about half of the rotational speed, r_e and L_e are the radius and depth of recrystallized zone. The depth of recrystallized zone is taken as thickness of material which went through dynamic recrystallization. For a given rotational speed, R_m is constant which is 12.5 rps for 1500 RPM. At edge, r_e is equivalent to radius of the rod (8.25 mm, half of rod diameter) and 0.1 mm for center. The depth of recrystallized zone is measured using optical micrograph, 2200 μm and 350 μm is obtained for edge and center location, respectively and marked in Fig. 6. By plugging these values, a strain rate of 294 s^{-1} and 22 s^{-1} are obtained for edge and center location, respectively. The calculated strain rate for edge location also matched perfectly well with the predicted strain rate. Further, the calculated strain rate from the analytical model is used to predict the correct temperature from the simulation. Keeping the strain rate equal to calculated from analytical model, grain size of 1.4 μm equivalent to experimental (Fig. 7(b)) is achieved at a temperature of 1323 K as shown in Fig. 9(b). The difference of 150 K is noticed from edge to center of the weld which also satisfy the general agreement that frictional heat is more if the surface area is large.

To confirm the feasibility of this model, simulation was also carried out to predict the strain rates for friction welds generated with 1200 and 1800 RPM. Fig. 10 represents the EBSD maps of

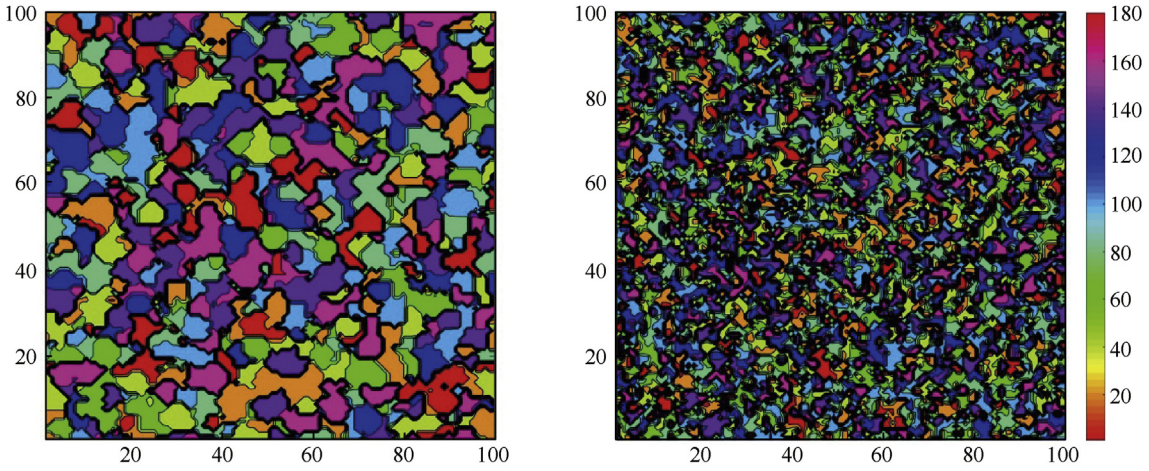

(a) 1 500 RPM: Edge

T: 1 473K, SR: 294 (1/s), GS: 2.97±0.23μm

(b) 1 500 RPM: Center

T: 1 323K, SR: 22.4 (1/s), GS: 1.40±0.02μm

Fig. 9. Simulated microstructure at 1473 K and (a) 294 s^{-1} and (b) 22 s^{-1} for edge and center, respectively.

friction welds generated with 1200 and 1800 RPM. For both center and edge locations, similar trends in grain size were observed for samples with 1200 and 1800 RPM as was observed for 1500 RPM. The average value of grain size at different locations is listed in Table 3. Depth of recrystallization and hardness value corresponding to that location is also listed in Table 3. It can be seen from Fig. 10 and Table 3 that central portion of friction welds went through higher amount of grain refinement as compared to edge in all the cases and validated by their corresponding hardness values.

Variation in grain size with respect to rotational speed is very small. For example, at the edge of the weld, the average grain size for 1200 RPM sample is 3.2 μm whereas for 1800 RPM sample, it is

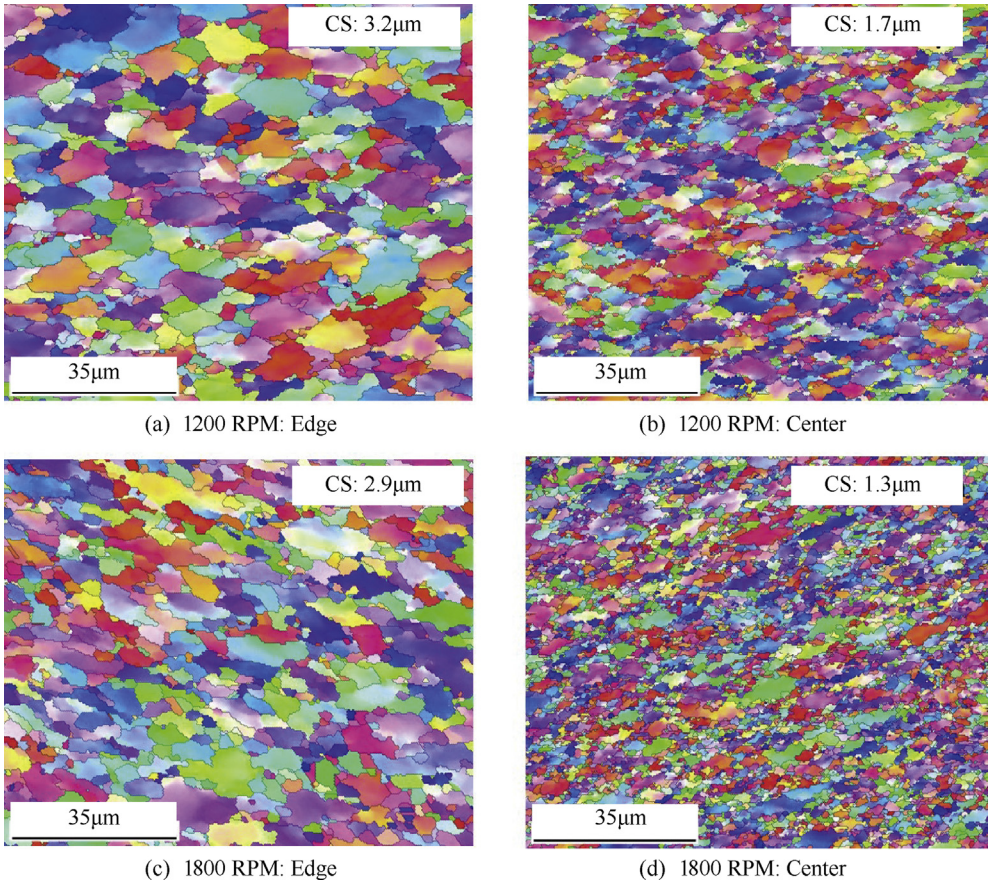

(a) 1200 RPM: Edge

(b) 1200 RPM: Center

(c) 1800 RPM: Edge

(d) 1800 RPM: Center

Fig. 10. EBSD maps of friction welds at (a) edge and (b) center generated with 1200 RPM and (c) edge and (d) center generated with 1800 RPM.

Table 3
List of depth of recrystallization, hardness values, grain size and calculated strain rate at center and edge of weld with different rotational speed.

RPM	$R_m/2$	r_e/mm	L_e/μm	Calculated strain rate/s^{-1}	Hardness/$HV_{0.3}$	Grain size/μm
1200	10	8.25 (Edge)	~2100	246.7	313.356	3.2
1200	10	0.1 (Center)	~423	14.85	381.6391	1.7
1500	12.5	8.25 (Edge)	~2200	294.37	302.1396	3.1
1500	12.5	0.1 (Center)	~350	22.43	421.8447	1.4
1800	15	8.25 (Edge)	~2000	388.57	302.0692	2.9
1800	15	0.1 Center)	~300	31.4	422.8921	1.3

2.9 μm. The difference in grain size is very small but show significant difference in strain rates as listed in Table 3. The calculated strain rate, based on equation (17), does not incorporate the temperature affect, therefore simulation was also run to check the strain rates for 1200 and 1800 RPM.

By keeping the temperature at 1473 K, simulations were run at 246 s^{-1} and 389 s^{-1} for 1200 and 1800 RPM, respectively. Grain size of 3.35 and 2.75 μm was achieved at 246 s^{-1} and 389 s^{-1} strain rates, respectively as shown in Fig. 11(a) and (c). The results matched almost closely with the experimental result, suggesting the temperature achieved during friction welding is almost identical for all the three rotational speeds. Identical temperature for all the rotational speed implying that once the material is plastically deformed, they achieve the steady stage temperature during friction welding. This type of phenomena is also observed in friction stir welding process which shows that for continuous generation of heat, a dynamic balance is required between contact stress and material yield shear stress [2,33]. Similarly, the strain rates were also predicted for center location. In this case also, strain rates almost similar to analytical strain rates matched the grain size for both 1200 and 1800 RPM welds at 1323 K as shown in Fig. 11(b) and (d). Identical temperature at all the RPM confirming the achievement of steady stage temperature during friction welding once it is plastically deformed. Temperatures of 1323 K ($0.78T_m$) and 1473 K ($0.89T_m$) are achieved at center and edge of the weld, respectively with 150 K difference from center to edge.

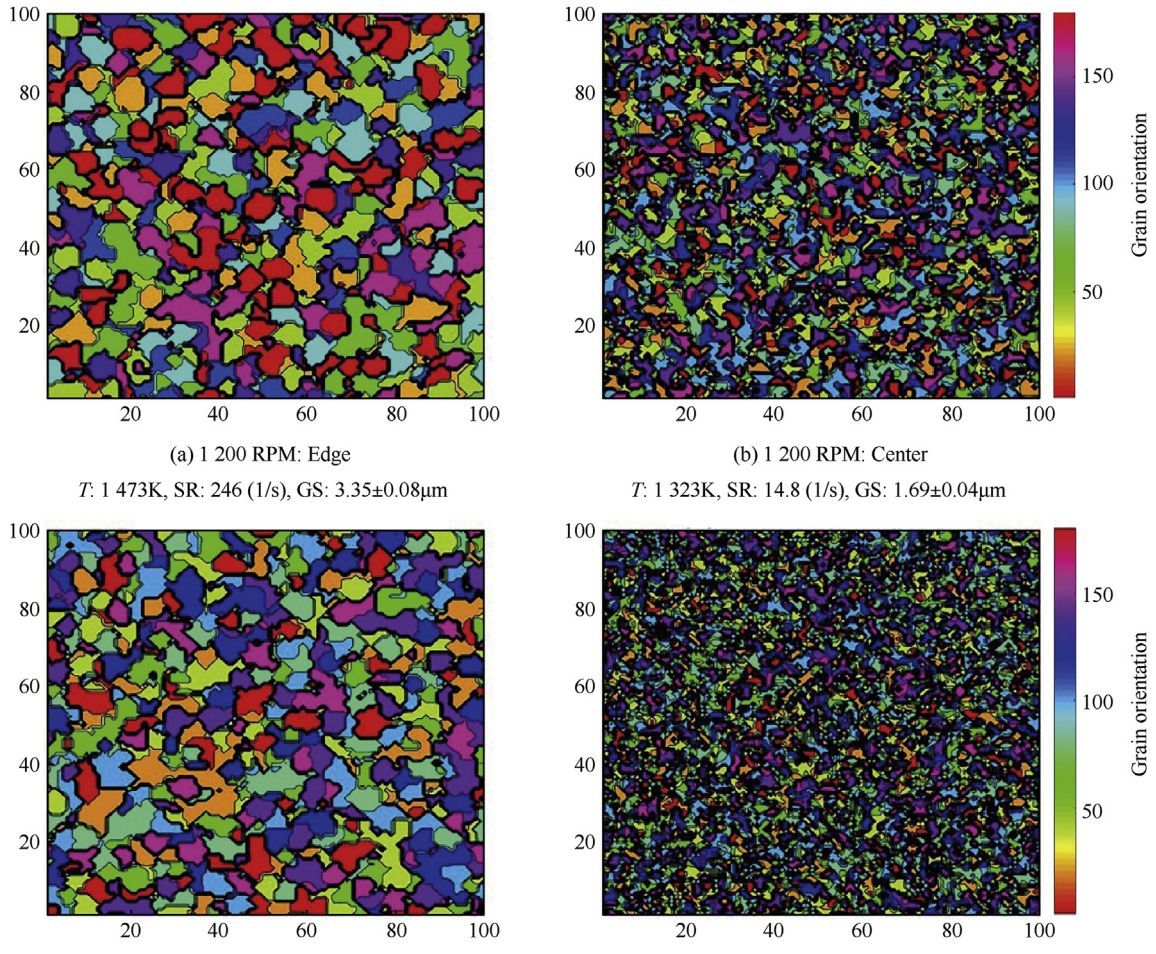

(a) 1 200 RPM: Edge
T: 1 473K, SR: 246 (1/s), GS: 3.35±0.08μm

(b) 1 200 RPM: Center
T: 1 323K, SR: 14.8 (1/s), GS: 1.69±0.04μm

(c) 1 800 RPM: Edge
T: 1 473K, SR: 388 (1/s), GS: 2.74±0.1μm

(d) 1 800 RPM: Edge
T: 1 323K, SR: 31.4 (1/s), GS: 1.29±0.02μm

Fig. 11. Simulated microstructure at (a) 1473 K/246 s^{-1}, (b) 1323 K/14.8 s^{-1}, (c) 1473 K/388 s^{-1} and (d) 1323 K/31.4 s^{-1}.

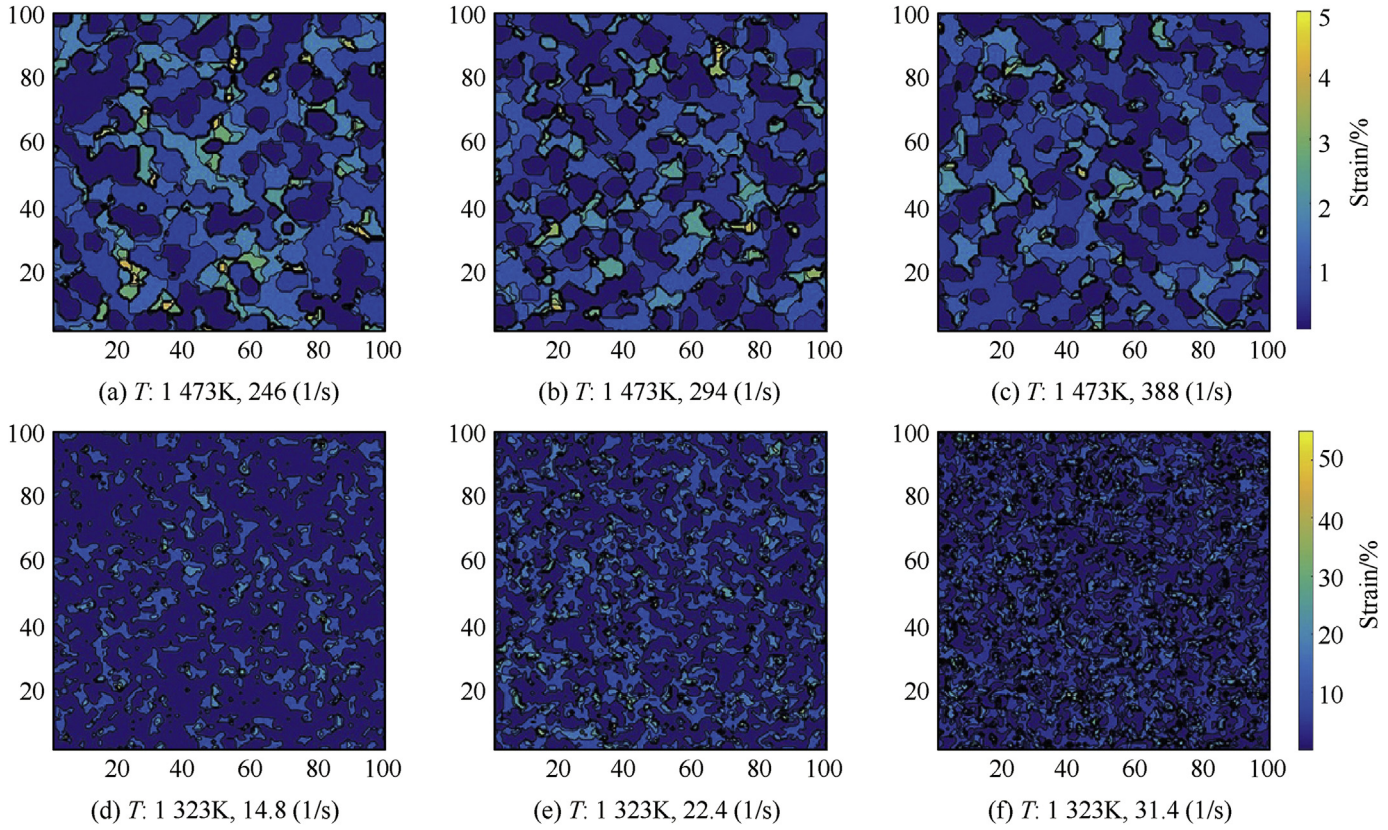

Fig. 12. Strain maps for edge location of the welds generated at (a) 1200, (b) 1500, and (c) 1800 RPM and center location at (d) 1200, (e) 1500, and (f) 1800 RPM.

4.3. Strain map

Using all the predicted strain rates and temperatures for the welds generated at three rotational speeds (1200, 1500, and 1800 RPM), strain maps were plotted after the final deformation as shown in Fig. 12. Fig. 12(a), (b), and 12(c) corresponds to the edge location of a weld generated at 1200, 1500, and 1800 RPM, respectively. In a same way, Fig. 12(d), (e), and 12(f) corresponds to the center location of a weld generated at 1200, 1500, and 1800 RPM, respectively. It can be observed from the overall results that at high temperature, the amount of strain accumulation is less compared to low temperature. For example, at 1473 K, the strain accumulation is 5% as comparted to 50% at 1323 K. The maximum intensity corresponds to those grains which are mostly non-recrystallized grains and present in very less quantity. Another observation is that at low temperature and low strain rate, the distribution of low strained grains (Fig. 12(d)) is higher compared to material deformed at high strain rate (Fig. 12(f)). On the other hand, at high temperature (1473 K), the strain distribution is almost uniform for all the strain rates. Overall the strain distribution map could be important data to figure out the correct temperature and time for the heat treatment process. The output of this data could be used as the input data for heat treatment grain growth model. It can be concluded that using this model localized strain rates, temperature, and induced strain in the microstructure can be calculated if one of parameter such as temperature and strain rate is known. In other way, a process map can be developed which will be used to get the strain rates and temperatures a material went through during any hot deformation process, if the resultant grain size is already known from the experiment.

5. Conclusions

Cellular automata based microstructure model has been developed to simulate microstructural evolution of Inconel 718 during hot deformation. Flow curves and grain sizes obtained from experiments and simulations were found to be quite comparable. Following are the key findings from this work:

1. In simulated flow curves, small deviation in later stages of deformation was observed which was attributed to adiabatic heating of material due to plastic deformation.
2. Larger grain size was observed at low strain rates and high temperatures attributed to more deformation time and higher grain mobility.
3. The strain rates predicted from simulation for both center and edge location of the weld were found to be increasing with increasing rotational speed.
4. Temperature difference of 150 K from center to edge of the welds was observed from the simulation result.
5. The simulated results showed that temperature tend to reach at steady state (0.78 Tm: center and 0.89 Tm: edge) for all the RPMs.
6. Higher amount of strain accumulation was noticed at low deformation temperature as compared to high deformation temperature.
7. Uniform strain distribution is observed at higher temperature for all the rotational speeds.

Acknowledgement

The authors would like to acknowledge Dr. Sekhar Rakurty and Dr. Deepankar Pal for their valuable suggestions in developing this model.

References

[1] Uday MB, Ahmad Fauzi MN, Zuhailawati H, Ismail AB. Advances in friction welding process: a review. Sci Technol Weld Join 2010;15:534–58. https://doi.org/10.1179/136217110X12785889550064.
[2] Nandan R, DebRoy T, Bhadeshia HKDH. Recent advances in friction-stir welding - process, weldment structure and properties. Prog Mater Sci 2008;53:980–1023. https://doi.org/10.1016/j.pmatsci.2008.05.001.
[3] Mishra RS, Ma ZY. Friction stir welding and processing. Mater Sci Eng R Rep 2005;50:1–78. https://doi.org/10.1016/j.mser.2005.07.001.
[4] Maalekian M. Friction welding – critical assessment of literature. Sci Technol Weld Join 2007;12:738–59. https://doi.org/10.1179/174329307X249333.
[5] Magudeeswaran G, Balasubramanian V, Madhusudhan Reddy G. Effect of welding processes and consumables on fatigue crack growth behaviour of armour grade quenched and tempered steel joints. Def Technol 2014;10:47–59. https://doi.org/10.1016/j.dt.2014.01.005.
[6] Kumar PV, Reddy GM, Rao KS. Microstructure, mechanical and corrosion behavior of high strength AA7075 aluminium alloy friction stir welds – effect of post weld heat treatment. Def Technol 2015;11:362–9. https://doi.org/10.1016/j.dt.2015.04.003.
[7] Mannan SL, Laha K. Creep behavior of Cr-Mo steel weldments. Trans Indian Inst Met 1996;49:303–20.
[8] Satyanarayana VV, Reddy GM, Mohandas T. Dissimilar metal friction welding of austenitic-ferritic stainless steels. J Mater Process Technol 2005;160:128–37. https://doi.org/10.1016/j.jmatprotec.2004.05.017.
[9] Neto DM, Neto P. Numerical modeling of friction stir welding process: a literature review. Int J Adv Manuf Technol 2013;65:115–26.
[10] Tutum CC, Hattel JH. Numerical optimisation of friction stir welding: review of future challenges. Sci Technol Weld Join 2011;16:318–24.
[11] He X, Gu F, Ball A. A review of numerical analysis of friction stir welding. Prog Mater Sci 2014;65:1–66. https://doi.org/10.1016/j.pmatsci.2014.03.003.
[12] Arora A, Zhang Z, De A, DebRoy T. Strains and strain rates during friction stir welding. Scr Mater 2009;61:863–6. https://doi.org/10.1016/j.scriptamat.2009.07.015.
[13] Song KK, Dong ZB, Fang K, Zhan XH, Wei YH. Cellular automata modelling of dynamic recrystallization microstructure evolution during friction stir welding of titanium alloy. Mater Sci Technol 2014;30:700–11.
[14] Asadi P, Kazem M, Givi B, Akbari M. Microstructural simulation of friction stir welding using a cellular automaton method: a microstructure prediction of AZ91 magnesium alloy. Int J Mech Mater Eng 2015. https://doi.org/10.1186/s40712-015-0048-5.
[15] Valvi SR, Krishnan A, Das S, Narayanan RG. Prediction of microstructural features and forming of friction stir welded sheets using cellular automata finite element (CAFE) approach. Int J Mater Form 2016;9:115–29. https://doi.org/10.1007/s12289-015-1216-0.
[16] Midling OT, Grong O. A process model for friction welding of AlMgSi alloys and AlSiC metal matrix composites-I. Haz temperature and strain rate distribution. Acta Metall Mater 1994;42:1595–609. https://doi.org/10.1016/0956-7151(94)90369-7.
[17] Rollett A. Overview of modeling and simulation of recrystallization. Prog Mater Sci 1997;42:79–99. https://doi.org/10.1016/S0079-6425(97)00008-X.
[18] Takaki T, Hirouchi T, Hisakuni Y, Yamanaka A, Tomita Y. Multi-phase-field model to simulate microstructure evolutions during dynamic recrystallization. Mater Trans 2008;49:2559–65. https://doi.org/10.2320/matertrans.MB200805.
[19] Ding R, Guo ZX. Coupled quantitative simulation of microstructural evolution and plastic flow during dynamic recrystallization. Acta Mater 2001;49:3163–75. https://doi.org/10.1016/S1359-6454(01)00233-6.
[20] Kugler G, Turk R. Modeling the dynamic recrystallization under multi-stage hot deformation. Acta Mater 2004;52:4659–68. https://doi.org/10.1016/j.actamat.2004.06.022.
[21] Chen XM, Lin YC, Wen DX, Zhang JL, He M. Dynamic recrystallization behavior of a typical nickel-based superalloy during hot deformation. Mater Des 2014;57:568–77. https://doi.org/10.1016/j.matdes.2013.12.072.
[22] Ding R, Guo ZX. Microstructural modelling of dynamic recrystallisation using an extended cellular automaton approach. Comput Mater Sci 2002;23:209–18. https://doi.org/10.1016/S0927-0256(01)00211-7.
[23] Estrin Y, Mecking H. A unified phenomenological description of work hardening and creep based on one-parameter models. Acta Metall 1984;32:57–70. https://doi.org/10.1016/0001-6160(84)90202-5.
[24] Humphreys FJ, Hatherly M. Recrystallization and related annealing phenomena. Elsevier Ltd; 2004.
[25] Mecking H, Kocks UF. Kinetics of flow and strain-hardening. Acta Metall 1981;29:1865–75.
[26] Zener C, Hollomon JH. Effect of strain rate upon plastic flow of steel. J Appl Phys 1944;15:22–32. https://doi.org/10.1063/1.1707363.
[27] Roberts W, Ahlblom B. A nucleation criterion for dynamic recrystallization during hot working. Acta Metall 1978;26:801–13.
[28] Weis MJ, Mataya MC, Thompson SW, Matlock DK. The hot deformation behavior of an as-cast alloy 718 ingot. Min Mater Mat. Soc 1989:135–54. https://doi.org/10.7449/1989/Superalloys_1989_135_154.
[29] Akram J, Dilip JJS, Pal D, Stucker B, Kalvala PR, Misra M. Microstructures of friction surfaced coatings – a TEM Study. Pract. Metallogr. 2016;53:261–72.
[30] Akram J, Puli R, Kalvala PR, Misra M. Microstructural studies on friction surfaced coatings of Ni-based alloys. Pract. Metallogr. 2015;52:590–606.
[31] Chang CI, Lee CJ, Huang JC. Relationship between grain size and Zener–Holloman parameter during friction stir processing in AZ31 Mg alloys. Scr Mater 2004;51:509–14. https://doi.org/10.1016/j.scriptamat.2004.05.043.
[32] Chang CI, Du XH, Huang JC. Achieving ultrafine grain size in Mg-Al-Zn alloy by friction stir processing. Scr Mater 2007;57:209–12. https://doi.org/10.1016/j.scriptamat.2007.04.007.
[33] Schmidt HB, Hattel JH. Thermal modelling of friction stir welding. Scr Mater 2008;58:332–7. https://doi.org/10.1016/j.scriptamat.2007.10.008.